Journal of Magnetic Resonance 281 (2017) 151–161

Contents lists available at ScienceDirect

Journal of Magnetic Resonance

journal homepage: www.elsevier.com/locate/jmr

Improvements, extensions, and practical aspects of rapid ASAP-HSQC and ALSOFAST-HSQC pulse sequences for studying small molecules at natural abundance

David Schulze-Sünninghausen [a,b], Johanna Becker [a], Martin R.M. Koos [a], Burkhard Luy [a,*]

[a] Institute of Organic Chemistry and Institute for Biological Interfaces 4 – Magnetic Resonance, Karlsruhe Institute of Technology (KIT), Fritz-Haber-Weg 6, 76131 Karlsruhe, Germany
[b] Bruker BioSpin GmbH, Rudolf-Plank-Str. 23, 76275 Ettlingen, Germany

ARTICLE INFO

Article history:
Received 30 March 2017
Revised 17 May 2017
Accepted 22 May 2017
Available online 24 May 2017

Keywords:
ASAP
HSQC
Fast NMR experiments
Steady state signal intensities
Polarization recovery
Non-uniform sampling
Broadband homouclear decoupling
BIRD
CLIP
Coupling constants
Shaped pulses
Water diluted samples

ABSTRACT

Previously we introduced two novel NMR experiments for small molecules, the so-called ASAP-HSQC and ALSOFAST-HSQC (Schulze-Sünninghausen et al., 2014), which allow the detection of heteronuclear one-bond correlations in less than 30 s at natural abundance. We propose an improved symmetrized pulse scheme of the basic experiment to minimize artifact intensities and the combination with non-uniform sampling to enable the acquisition of conventional HSQC spectra in as short as a couple of seconds and extremely ^{13}C-resolved spectra in less than ten minutes. Based on steady state investigations, a first estimate to relative achievable signal intensities with respect to conventional, ASAP-, and ALSOFAST-HSQC experiments is given. In addition, we describe several extensions to the basic pulse schemes, like a multiplicity-edited version, a revised symmetrized CLIP-ASAP-HSQC, an ASAP-/ALSOFAST-HSQC sequence with broadband BIRD-based ^{1}H,^{1}H decoupling, and a symmetrized sequence optimized for water suppression. Finally, RF-power considerations with respect to the high duty cycle of the experiments are given.

1. Introduction

Two-dimensional heteronuclear correlation experiments with good sensitivity such as the HSQC [2] (Heteronuclear Single Quantum Correlation spectroscopy) are workhorses of today's high-resolution NMR spectroscopy. Accelerated experiments like the SOFAST-HMQC [3–6], the BEST sequences [7–9], or the COST-HSQC [10] are known and routinely used for a decade in isotope-labeled samples. Analogous experiments at natural-abundance isotope level, however, are scarcely applied so far, although applications like metabolomics-type studies, reaction monitoring, and the analysis of unstable molecules would strongly benefit from corresponding experiments. The main reasons are certainly the conservatism of users and some of the drawbacks from most existing approaches.

Among the available techniques, the fastest acquisition of 2D experiments is certainly achieved via the ultrafast methodology, with which the spectrum can be obtained in a single scan using gradient-encoding imaging-type schemes [11–14]. The acquisition scheme, however, faces severe limits in accessible resolution, spectral width and sensitivity and is so far not suited for most routine small molecule applications.

A more straightforward method is based on the signal intensity optimization according to the so-called Ernst angle [15]. Among the reported techniques [3–8,16–20], the most promising ones are the ALSOFAST- [21] (ALternate SOFAST) and the ASAP-HMQC (Acceleration by Sharing Adjacent Polarization) [17] and their corresponding HSQC variants [1]. They allow the acquisition of 2D experiments with very short overall experiment time as well as the acquisition of 2D spectra with very high resolution in the indirect dimension within a reasonable time span. The experiments can be applied the same way as a conventional HSQC and enable the acquisition of ^{1}H,^{13}C correlation spectra with uncompromised quality.

Here, we introduce an improved symmetrized version of the ASAP-HSQC [1], as well as several extensions with respect to multiplicity editing, water suppression, the measurement of one-bond

* Corresponding author.
E-mail address: burkhard.luy@kit.edu (B. Luy).

http://dx.doi.org/10.1016/j.jmr.2017.05.012
1090-7807/

couplings, and the application of BIRD filter-based [22] pure shift spectra. In addition, general considerations concerning polarization recovery, sensitivity, and the application of non-uniform sampling (NUS) [23,24] for extremely short experiments and/or extremely well-resolved spectra are given. Furthermore, the use of broadband excitation, inversion, and refocussing pulses [25–33] to obtain highest possible robustness of the experiment and their impact on spectral quality is studied. Together with considerations concerning the applied rf-energy we provide a detailed characterization of possibilities and potential limitations of the ASAP and ALSOFAST techniques as widely applicable fast experiments for most natural abundance applications.

2. Basic pulse sequences

2.1. Symmetrized ASAP/ALSOFAST-HSQC

The ASAP and ALSOFAST approaches are based on the selective excitation of all ^{13}C-bound protons, while returning all unused magnetization from active and passive protons to z, providing a reservoir of spin polarization for the following scan. While the ALSOFAST approach essentially uses the reservoir as is with a dramatically reduced recovery delay, the distinctive ASAP feature is quick distribution of the reservoir over all protons including the ^{13}C-bound ones via a short homonuclear mixing period of approximately 40 ms. The originally reported pulse sequence (see Fig. S1 in the supporting information and Ref. [1]) works best if broadband shaped pulses are introduced that are especially needed for artifact-free coherence order selection. Fig. 1A shows a novel, symmetrized pulse sequence of the ASAP-HSQC [1] with a modified gradient scheme. The first gradient of the coherence order selection and echo/antiecho encoding is split into two gradients of equal sign and strength, which are applied directly before and after the t_1 evolution period. This way ^{1}H magnetization can be maintained in a gradient echo during t_1. The last 90° pulse on protons, which flips the magnetization of the passive proton spins into the z-direction, can then be applied directly at the beginning of the back transfer step equivalent to the conventional HSQC experiment. Coherence order selection is achieved by switching gradients according to $G_3/G_4 = \pm\gamma_H/(2 \cdot \gamma_c)$ due to the

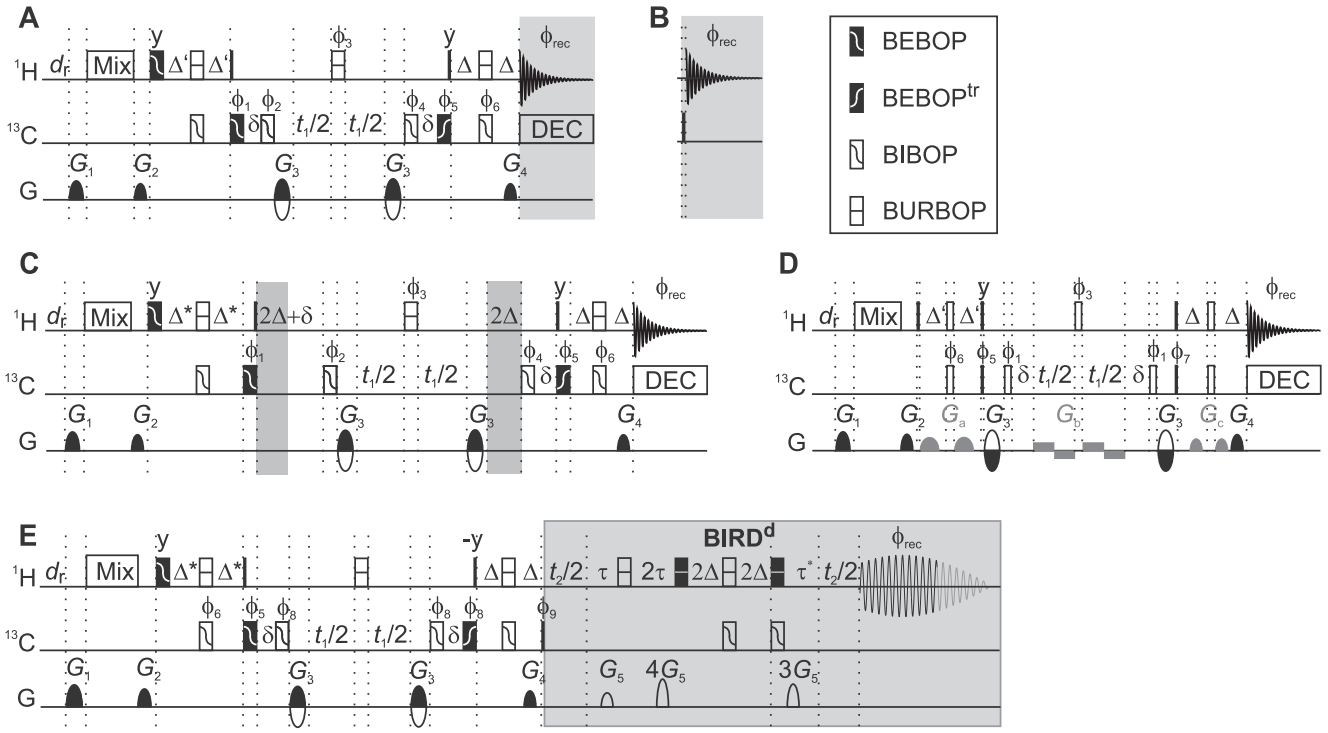

Fig. 1. Pulse sequences of the symmetrized ASAP-HSQC (A), the modification for the symmetrized CLIP-ASAP-HSQC (B), the multiplicity-edited ASAP-HSQC experiment (C), an ASAP-HSQC sequence with improved water suppression (D), and a pure shift ASAP-RESET-HSQC experiment with broadband homonuclear ^{1}H,^{1}H decoupling (E) are shown. The grey gradients in (D) lead to dephased water magnetization in the transverse plane to reduce radiation damping effects [34]. Pulse sequence elements in grey boxes emphasize modifications/extensions of the basic sequence. The ASAP-CLIP-RESET-HSQC (E) allows the accelerated acquisition of broadband ^{1}H,^{1}H-decoupled HSQC spectra as pseudo-3D interferogram. Pulse phases are x unless indicated otherwise. Vertical lines represent 90° hard, black boxes represent 90° broadband pulses. Narrow unfilled rectangles correspond to 180° hard and wide unfilled rectangles to 180° broadband pulses. Whenever possible, pulse sequences were implemented using broadband excitation/time-reversed excitation/inversion pulses from the BEBOP/BIBOP family [26–30,35] and universal rotation pulses from the BURBOP family [25,31,32] as depicted in the upper right part of the figure. Filled rectangles on the ^{1}H mark a BEBOP ($z \rightarrow -y$) (10 kHz, 20 kHz, 550 μs, ±20%, 1100) [33] pulse with excitation properties equivalent to an on-resonant 90°$_x$ hard pulse. Filled rectangles on the ^{13}C channel mark a BEBOP($z \rightarrow -y$) (37.5 kHz, 10 kHz, 550 μs, ±5%, 1100) (^{13}C) pulse or its time-reversed shape (tr), again equivalent to a 90°$_x$ hard pulse, using the nomenclature introduced in Ref. [25].For simultaneous refocusing on protons and broadband inversion on carbon coupling-compensated 600 μs BUBI pulse sandwiches for best overall performance were applied [33,36,37]. The proton pulse of the sandwich is also used as a BURBOP-180$_x$ (10 kHz, 20 kHz, 600 μs, ±20%, 1200) [33] while the ^{13}C pulse is also used as a BIBOP (37.5 kHz, 10 kHz, 600 μs, ±5%, 1200) [33]. All proton shaped pulses are applied with an rf-amplitude of 20 kHz, carbon shaped pulses with an rf-amplitude of 10 kHz. Although only a subset has been used for the experiments shown, full phase cycling is given by ϕ_1 = 4(x), 4(−x); ϕ_2 = 4(y), 4(−y); ϕ_3 = 2(x), 2(−x); ϕ_4 = 4(−y), 4(y); ϕ_5 = x, −x; ϕ_6 = x; ϕ_7 = 4(x), 4(−x); ϕ_8 = 2(x), 2(−x); ϕ_9 = x, −x; ϕ_{rec} = x, −x, x, −x, −x, x, −x, x (A to D); and ϕ_{rec} = x, −x, −x, x (E). The delay $\Delta = 1/(4 \cdot {}^1J_{CH})$ is typically set to an average coupling constant of 145 Hz, while Δ' or Δ^* are optimized individually for every sample as an equivalent to Ernst angle excitation [15]. The delay δ is used to refocus unwanted coupling and chemical shift evolution during t_1, rf-pulses, and gradients. Heteronuclear decoupling was achieved using GARP [38], but more efficient decoupling schemes may be applied. The rectangle with the insert Mix indicates an isotropic mixing scheme which was implemented either using the DIPSI-2 sequence [39] or the MOCCA-XY16 sequence [40,41]. In the ALSOFAST-HSQC, the mixing sequence is replaced by a conventional recovery delay. Purge gradients were set to G_1 = 43%, G_2 = 33%, G_5 = 17%, G_a = 90%, G_c = 90%, and G_b = 2% of the maximum gradient strength of 50.7 G/cm. Echo/antiecho and coherence order selection was achieved by switching gradients according to G_3 = (40%, −40%), G_4 = (20.1%, 20.1%). Phase-sensitive detection in the indirect dimension using TPPI [42] was achieved by simultaneous inversion of phases ϕ_5 and ϕ_6.

addition of the two gradients G_3 with same sign. The pulse scheme allows the application of Ernst angle type excitation by optimizing the delay Δ' in the INEPT as reported for the ALSOFAST-HMQC [21]. While well-known DIPSI-2 [39] or MOCCA-XY16 [40,41] mixing sequences are applied in the ASAP variants [43], a short recovery delay is applied in analogous ALSOFAST experiments. Pulse sequences in Fig. 1B–E represent modified or extended schemes based on the symmetric ASAP-HSQC scheme. With the CLIP-ASAP-HSQC (Fig. 1B), pure inphase ω_2-coupled ^{1}H,^{13}C correlation spectra for one bond coupling measurement are obtained. The sequence in Fig. 1C displays a multiplicity-edited ASAP-HSQC and the sequence in Fig. 1D is optimized for effective water suppression. Finally, Fig. 1E shows the pure shift CLIP-ASAP-RESET-HSQC sequence with broadband homonuclear ^{1}H,^{1}H decoupling in the proton dimension. Decoupling is achieved by recording individual chunks of an interferogram in a pseudo dimension. All modified and extended experiments will be explained in more detail in Section 5.

2.2. Symmetrized vs. original ASAP-HSQC

In line with the already published ASAP-HSQC, we optimized the sequence using broadband BEBOP [26–30], BURBOP [25,31,32], and BUBI [33,36] shaped pulses for improved robustness and sensitivity as described in more detail in the caption of Fig. 1.

In the original sequence using hard pulses, peak doubling at ^{13}C frequencies shifted by half the spectral width has been observed, especially for very short experiments with one scan per t_1 increment. The primary source of such shifts most likely is the TPPI method applied with imperfect pulses. In the original sequence coherence order selection and echo/antiecho detection is only achieved by a change in coherence order of the carbon magnetization with low gyromagnetic ratio, while the symmetrized version allows the application of the well-proven coherence order selection scheme of conventional echo/antiecho-encoded HSQC sequences. With the symmetrized version of the ASAP-HSQC (Fig. 1A), therefore, a reduction of artefact peaks is achieved. The comparison of the two ASAP-HSQC sequences is illustrated in Fig. 2, together with a comparison of the performance of hard and the Optimal Control Theory-derived broadband pulses. Using no additional interscan delay d_1, an ASAP-HSQC in each case was recorded in less than 30 s. As can be seen, the application of conventional hard pulses leads to artifact signals in the ^{13}C dimension, especially in the original version of the experiment. The artifacts are significantly reduced in the symmetrized version, but still visible as long as hard pulses are used. The sequences were significantly further improved using broadband BEBOP [26–30], BURBOP [25,31,32], and BUBI [33,36] shaped pulses for improved robustness and sensitivity as described in the original ASAP-HSQC publication [1] and in the caption of Fig. 1. For both sequences with broadband shaped pulses artifact signals essentially vanish in resulting spectra.

A detailed examination revealed that the sensitivity of the original ASAP-HSQC sequence for some samples is higher by a few percents compared to the symmetrized sequence, which can be explained by the shorter timespan the reservoir magnetization spends in the transverse plane. Thus the loss of reservoir magnetization as a result of evolving ^{1}H,^{1}H couplings and transverse relaxation is smaller in the original version of the sequence. In terms of artifact signals, however, the spectral quality of the symmetrized sequence is noticeably higher with better-defined line shapes in the ^{13}C dimension. Especially in combination with non-uniform sampling (*vide infra*) the benefits in this regard become pronounced.

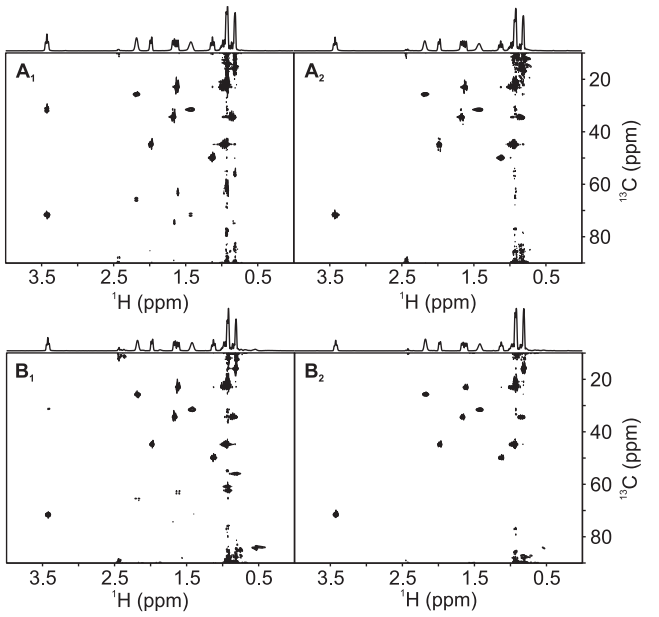

Fig. 2. HSQC spectra of menthol in $CDCl_3$ acquired using the original ASAP-HSQC sequence (see Ref. [1] and Fig. S1) (A_1 and A_2) and the symmetrized ASAP-HSQC shown in Fig. 1A (B_1 and B_2). Spectra with subscript index 1 were recorded using hard pulses, while the index 2 indicates the application of Optimal Control-derived broadband pulses. The spectra were recorded with 512 × 128 data points, corresponding to acquisition times of 106.8 and 5.3 ms for the two dimensions. 1 scan per t_1 increment and 16 dummy scans in 23 s were performed for each experiment. While artifact signals are visible in the hard pulse versions, best, almost artifact-free spectra are obtained for B_2.

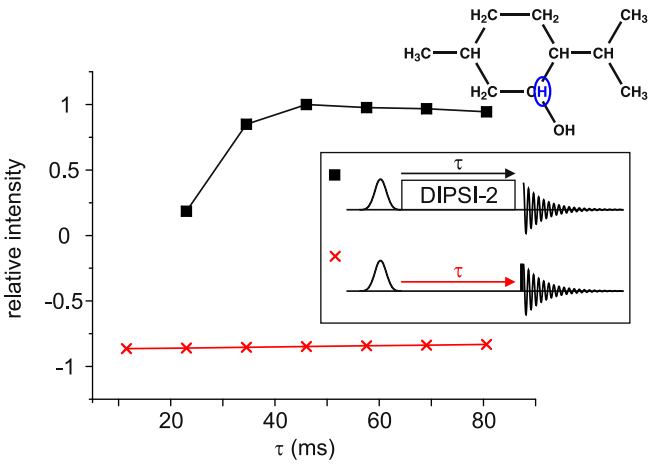

Fig. 3. Experimental verification of the difference in polarization recovery using a simple recovery delay (red crosses) and isotropic mixing with a spin reservoir (black boxes). The highlighted proton of menthol was inverted using a band selective rf-pulse before recovery. Surrounding protons, in this case, serve as the polarization reservoir. Clearly, the tremendous acceleration of polarization recovery can be seen.

3. Signal intensity considerations

3.1. ASAP-enhanced recovery

As mentioned before, the pulse sequence of the ALSOFAST-HSQC basically equals the sequence of the ASAP-HSQC, with the difference that the mixing period is replaced by a conventional recovery delay. While the advantages from Ernst angle-type excitation remains, the sensitivity enhancement due to the mixing step does not. Figure 3 shows the comparison of the recovery of the two experimental schemes. Two different selective inversion

recovery experiments were performed to simulate the recovery after a single scan in the HSQC experiments. Clearly, for the studied small molecule menthol, the mixing sequence leads to a much faster recovery of the *z*-magnetization of the selectively inverted proton spin. Indeed, especially in very short experiments on small molecules the ASAP approach leads to significant signal enhancements when reservoir spins are accessible via couplings. For larger molecules, however, the ALSOFAST scheme may be preferable due to lower rf-power input and relaxation losses during the mixing step for molecules with higher molecular weights and thus shorter transverse relaxation times T_2.

For longer experiments with many increments, it has to be taken into account that also the magnetization reservoir will eventually be depleted. Thus, the build-up curve of Fig. 3 should only be taken as an estimate for very short HSQC experiments. The steady-state case, which is relevant for longer overall experiment times, is briefly discussed in the following section.

3.2. Comparison of steady-state signal intensities

NMR experiments often feature not just a single acquisition but repeated pulsing and acquisition in rapid succession, i.e. increments in 2D experiments or scans in 1D and 2D experiments, without intermediate complete relaxation of the sample spins to the equilibrium state. The system will initially yield fluctuating signals, but will stabilize into a *steady state* after a sufficient number of repetitions. Disregarding instrumental instability, this steady state will provide identical signals for each repetition and has to be investigated to understand the relaxation behavior of the new experiments. Based on the well-known saturation-recovery experiments utilized to measure T_1 relaxation, an HSQC-recovery experiment was devised and performed on menthol in $CDCl_3$ covering a large parameter space. The measured data are evaluated to quantify the signal-to-noise ratio to be expected from the conventional, ALSOFAST-, and ASAP-HSQC under the steady-state condition of 2D experiments with many scans.

The experiment consists of a series of 1D-HSQC elements. A preparation HSQC block including an incremented recovery delay τ_{rec} is repeated 64 times followed by a readout HSQC element. The pulse sequence is based on the pulse sequence shown in Fig. 1A and it is sketched in Fig. 4A. (For the exact layout please see the supporting information.)

The preparation HSQC contains two INEPT steps. The delays Δ' of the first INEPT can be varied to achieve incomplete transfer in the CH_n spin systems. The remaining untransferred coherence from all protons (^{13}C-bound and others) can be returned to polarization after each scan to serve as a reservoir and the delay Δ′ serves as a flip angle equivalent for the ^{13}C-bound protons. The effective angle $\beta = 2\pi\ ^1J_{CH}\ \Delta'$ describes the phase angle between measurable magnetization and polarization. The delay of the second INEPT step was $\Delta = (4 \cdot 145\ \text{Hz})^{-1}$ throughout the experiment, while Δ′ was varied from 0.1 Δ to 1 Δ.

Depending on a single pulse phase in the preparation HSQC, the reservoir of untransferred magnetization is either dephased to recreate the state corresponding to the conventional experiment (nullifying any advantage from reduced flip angle or transfer delay) or preserved to create ALSOFAST conditions. For ASAP-like conditions, a 34.5 ms DIPSI-2 mixing sequence is included after the recovery delay τ_{rec} and before the first pulse of the next HSQC element. After 64 repetitions of the preparatory block, the system is assumed to be sufficiently close to the steady state. For the readout HSQC, both transfer delays were set to $\Delta = (4 \cdot 145\ \text{Hz})^{-1}$. The readout signal is proportional to the steady state polarization; integrating and normalizing with respect to a fully relaxed experiment ($\tau_{rec} = 10$ s) yields the normalized steady state polarization P_n, the basis for the following evaluation.

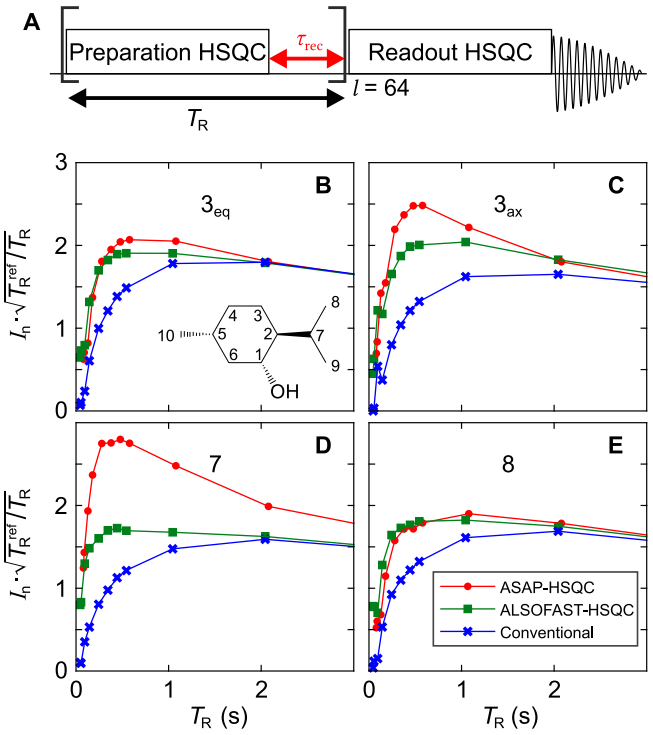

Fig. 4. Experimental comparison of signal-to-noise ratios between conventional HSQC, ALSOFAST-, and ASAP-HSQC experiments. (A) Sketch of the HSQC-recovery pulse sequence used to measure the steady state polarization and polarization recovery. (B–E) Experimental normalized steady-state signal intensity I_n of a single scan per square root of the duration T_R. The INEPT delay Δ′ was optimized for maximum overall intensity for each experiment and recovery delay τ_{rec} or T_R. Four signals of menthol in $CDCl_3$ are shown. The equatorial 3_{eq} proton (B) has a large coupling to the 3_{ax} proton but only small coupling constants to the surrounding ring protons (ddddd, J_{HH} = 12.8 Hz, 3.3 Hz, 3.3 Hz, 3.3 Hz, 2.1 Hz). The axial 3_{ax} proton (C) has large coupling constants not only to the geminal proton but to the surrounding axial protons as well (dddd, J_{HH} = 12.8 Hz, 12.8 Hz, 11.7 Hz, 3.5 Hz). The proton at the 7-position (D) is coupled to two methyl groups and ring protons that are providing a large reservoir (qqd, J_{HH} = 7 Hz, 7 Hz, 2.8 Hz). The methyl group at the 9-position (E) consists of three active protons coupled to a single reservoir spin (d, J_{HH} = 7 Hz), reducing the influence of the reservoir. In a real experiment, T_R must include the 10–30 ms duration of the pulse sequence, the mixing sequence when applicable, and the acquisition time, which is usually limited to 0.1–0.4 s by probehead specifications concerning decoupling power. Therefore, for most small molecules with relaxation time T_1 of one to two seconds, the maximum signal-to-noise ratio in the ALSOFAST- and ASAP-HSQC coincides with typical acquisition times.

When the transfer delay Δ′ is reduced, the steady state polarization P_n is increased but the normalized steady state signal intensity I_n is reduced to $I_n = P_n \cdot \sin(2\pi\ ^1J_{CH}\ \Delta')$, depending on the one-bond coupling $^1J_{CH}$ (taken from Ref. [43]). For the conventional experiment, Δ′ = Δ was used, while the ALSOFAST- and ASAP-HSQC allow optimizing Δ′ for each value of τ_{rec} within the rather coarse set of 11 values of Δ′. Examples of polarization P_n and intensity I_n are shown in the supporting information.

To compare experiments of different length, a good property is the achievable signal-to-noise ratio per experiment duration. In our setup, this comparison is accomplished by dividing the single scan intensity I_n by the square root of the duration of a single scan T_R, normalizing by the length of the reference experiment (approximately 10 s). Fig. 4 shows the comparison for the signals of four different spins of menthol in $CDCl_3$. The T_1 relaxation times of all signals lie in the range of 1.5–2 s, and with repetition times T_R larger than T_1, the difference between the experiments becomes small. In this case, relaxation processes render the magnetization already close to equilibrium polarization, so that isotropic mixing and Ernst angle excitation represent only minor contributions.

For fast experiments and short recovery delays or repetition times T_R, however, the situation changes dramatically. Ernst angle-type excitation significantly enhances the signal intensities of all spins in the ALSOFAST-HSQC compared to the conventional HSQC experiment in Fig. 4.

With no coupled remote spins – i.e. without a reservoir accessible by isotropic mixing – the ASAP-HSQC provides no benefit compared to the ALSOFAST experiment but has two negative contributions: Firstly, the mixing sequence requires time that is not available for free T_1 relaxation, a consideration especially important in the fast pulsing regime. Secondly, the mixing sequence also has the effect of saturating the spins, reducing the available magnetization, which is relevant for all repetition times and spin systems. When polarization is shared between active and reservoir spins, however, the available polarization and therefore signal intensity is greatly increased in the ASAP case. The 3_{eq} and 3_{ax} protons (B and C) for example have the same effective spin system but significantly different coupling constants to the other ring protons. Consequently, 3_{ax} shows greatly increased intensity in the ASAP-HSQC while 3_{eq} only shows a moderate increase in S/N due to the smaller overall coupling constants. The proton at 7 is adjacent to two methyl groups, and shows increased intensity. The methyl group at position 8, instead, contains three active spins but only one adjacent proton, therefore the ASAP-HSQC shows no measureable improvement over the ALSOFAST-HSQC. In general, the mixing efficiency depends on the homonuclear coupling constants [44–49] and results are hard to predict, but the signal intensities in Fig. 4 clearly show, the more spins are accessible as spin reservoir in the ASAP experiment, the higher will be the gain in signal-to-noise ratio.

It should be noted that in the full 2D-HSQC experiment, the acquisition time in the directly detected ω_2 dimension is part of the length of a single scan T_R. On the one hand, this poses a severe restriction when shortest overall experiment times are to be achieved; on the other hand, HSQC experiments with broadband heteronuclear decoupling are usually recorded with acquisition times ranging between 50 and 400 ms, which leads to recovery times with maximum gain in sensitivity for the ASAP and ALSOFAST approaches.

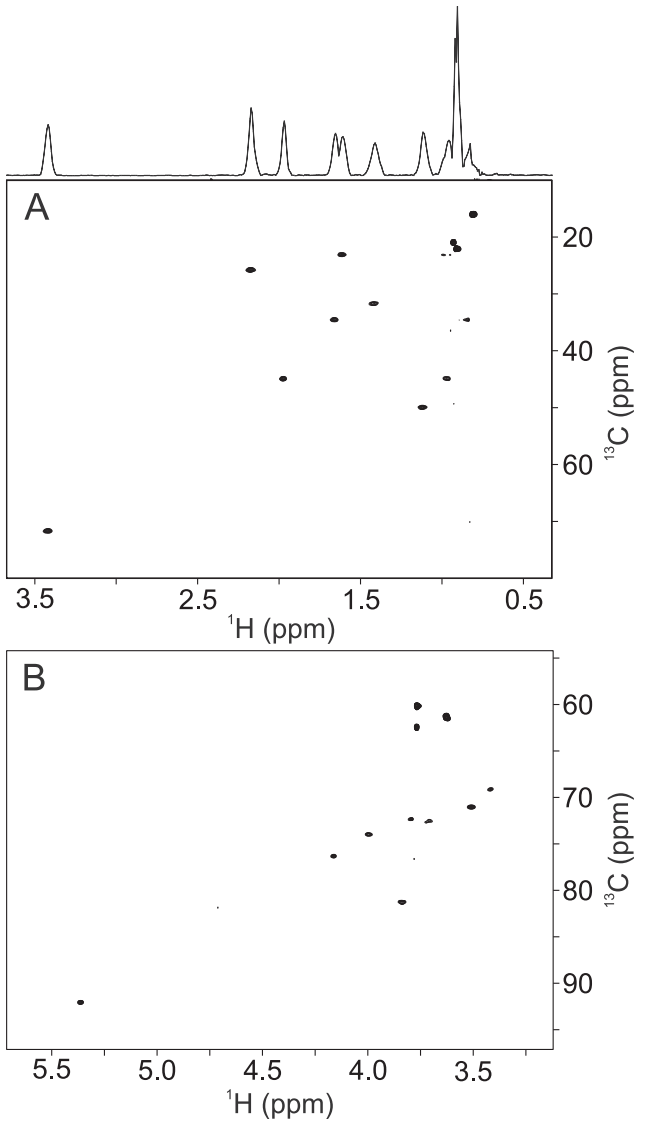

Fig. 5. HSQC spectra of a 500 mM menthol sample (A) in $CDCl_3$ and a 10 mM sucrose sample (B) in D_2O using the symmetrized $^{1}H,^{13}C$-ASAP-HSQC optimized for minimum overall experiment time. Spectrum A was recorded using an expanded 256 × 128 matrix of real data points with acquisition times of 53.4 ms and 5.3 ms, respectively. One scan per t_1 increment and 4 dummy scans at the beginning of the experiment were performed with an ASAP isotropic mixing period of 11.5 ms. The actually acquired amount of data points in the indirect dimension was reduced to 18 increments using NUS. The overall experiment time was 1.9 s. Spectrum B was recorded using an expanded 268 × 128 matrix of real data points with acquisition times of 74.5 ms and 8.5 ms, respectively. One scan per t_1 increment and 4 dummy scans at the beginning of the experiment were performed with an ASAP isotropic mixing period of 11.5 ms. The actually acquired amount of data points in the indirect dimension was reduced to 24 increments using NUS. The overall experiment time was 2.9 s.

4. ASAP-HSQC and non-uniform sampling

4.1. Minimal experimental times

In contrast to the ultrafast approach, the ASAP-HSQC experiment can be easily combined with other techniques for reduced overall measurement time such as non-uniform sampling (NUS) [23,24]. In this combination, the ASAP-HSQC allows the acquisition of extremely fast HSQC experiments: With NUS applied to typical small molecules the number of actually acquired t_1 increments can be reduced from 128 to only 18 without loss in information content; together with optimized FID durations this results in an overall experiment time of about two seconds. Fig. 5A shows a corresponding fast experiment acquired on menthol as a quite difficult test sample with strong coupling contributions and a large dynamic range from very intensive methyl signals directly next to very broad methylene multiplets. The experiment acquired in 1.9 s provides a complete and clean spectrum in which all correlations can be identified. Using a conventional HSQC sequence, it is not possible to acquire a spectrum in a similar time (see Fig. S2 in the supporting information for comparison).

With this extremely fast correlation experiment the ASAP-HSQC does not fully approach the speed of ultrafast experiments that record spectra in a single scan, therefore providing acquisition times even below one second. For many applications, however, the acquisition of spectra with measurement times of about two seconds are equally feasible. In such cases, the ASAP-HSQC provides a significantly higher signal-to-noise ratio: while the signal intensities acquired by the ASAP-HSQC and the ultrafast approach will be roughly proportional to the square root of overall measurement time [50], the acquired noise is mainly determined by the different filter widths used in the specific experiments. A four-fold filter width, for example, doubles the acquired noise via folding. While the ASAP-HSQC can be acquired with ideal filter widths matching the dwell time and thereby leading to minimal noise contributions, the situation in the ultrafast is very different, as

filter widths are not determined by the dwell time, but by the repetition rate of points acquired for the *k*-space dimension.

The good achievable signal-to-noise-ratio of the ASAP-HSQC leads to heteronuclear correlations of good quality even in the case of natural abundance samples at low concentrations. As shown in Fig. 5B on sucrose in D_2O using a cryogenically cooled probehead, an ASAP-HSQC on a 10 mM sample can be acquired in 2.9 s, and samples with 2 mM concentration are detectable with measurement times of 15 s (Fig. 8 in Section 5) as long as the NUS-based reduction of t_1 increments applies.

4.2. Maximum resolution

In a previous publication we could show that a $^1H,^{13}C$ spectrum of maltose could be acquired with a digital resolution of 0.54 Hz in the indirect dimension in only 3 h using the ASAP approach. The resolution allowed to even distinguish the signals of α- and β-maltose for Carbons 9 and 11 which are approximately 3 Hz apart in both cases. For the spectrum, the full number of t_1 increments was acquired. It is, however, possible to reduce the number of acquired increments greatly by utilizing a combination of NUS, zero filling, and linear prediction to acquire a spectrum with extreme digital resolution in the indirect dimension significantly below 1 Hz in an overall experimental time of approximately 7 min. As previously reported for the 3 h experiment, the possibility to distinguish α- and β-maltose from Carbons 9 and 11 is still retained in the short experiment as shown in Fig. 6. The only drawback is the relatively long processing time of the NUS data with the still large number of t_1 increments used, which is on the order of hours on a 16 core PC.

The achievable resolution in a time span typical for conventional $^1H,^{13}C$-HSQC experiments opens the door to widespread applications. Comparing such a spectrum to a conventional 1D carbon spectrum with similar ^{13}C resolution acquired at the same experimental time, the sensitivity is significantly enhanced due to ^1H excitation and detection. Carbon chemical shift based metabolomics and/or fluxomics with resolved $^{13}C,^{13}C$ couplings of isotope-labeled compounds in the indirect dimension will be possible as well as significantly enhanced structure determination of repeating elements with only slight differences in carbon chemical shifts.

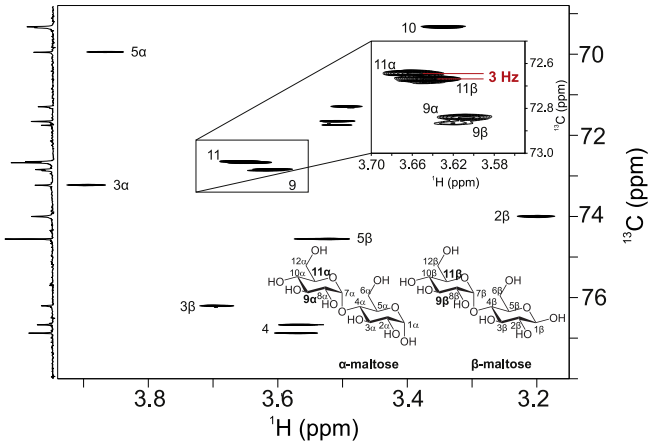

Fig. 6. $^1H,^{13}C$-ASAP-HSQC spectrum of a 200 mM maltose sample in D_2O. The spectrum was recorded with an expanded matrix of 256 × 8192 data points, corresponding to acquisition times of 71.2 and 452.6 ms for the two dimensions. Due to 15% NUS sampling the number of actually acquired points in the indirect dimension is reduced to 1228. The experiment was acquired using 1 scan per t_1 increment and 32 dummy scans in altogether 7 min and 14 s. The spectrum was processed using compressed sensing. In addition, linear prediction as well as zero filling with twice the time domain points in both dimensions was applied. The resulting digital resolution is 0.55 Hz in the carbon dimension. This high resolution allows the distinction of 9α/β and 11α/β of maltose, which both are approximately 3 Hz apart.

5. Experiment extensions

5.1. Multiplicity edited ASAP-HSQC

Multiplicity editing of CH_2 vs. CH and CH_3 groups in HSQC spectra gives very useful additional information at practically no cost [51–53]. This is achieved by simply adding a delay with total length of $4\Delta = 1/^1J_{CH}$, during which scalar $^1H,^{13}C$-couplings evolve while chemical shift evolution of the transverse ^{13}C spins is refocused. This approach can also be incorporated into the ASAP-HSQC scheme (Fig. 1C). However, the different transfer pathways, especially of spin reservoir magnetization, have to be taken into account. Proton magnetization that is coupled to ^{13}C spins but not transferred to carbons during the initial INEPT step due to Ernst angle-type coherence transfer will be inverted by the additional coupling delay. Protons not bound to ^{13}C, instead, also contribute to the polarization reservoir for the next scan, but are not inverted by the delay, resulting in opposite signs of the reservoir constituents. To still profit from effective Ernst angle excitation, the optimal steady state transfer is modified from $\beta' = 180° \cdot (^1J_{CH} \cdot 2\Delta')$ to $\beta^* = 180° \cdot (^1J_{CH} \cdot 2\Delta^*)$ using the delay $\Delta^* = 1/(2 \cdot {}^1J_{CH}) - \Delta'$, or equivalently, $\Delta^* = 2\Delta - \Delta'$. A graphical illustration of how the delay has to be adjusted is shown in Fig. S6 in the supporting information. The delay creates an additional selective 180° rotation only for the ^{13}C-bound proton magnetization corresponding to $\beta^* = 180° - \beta'$ and thus compensates the effect of the multiplicity-editing step.

For an ASAP-HSQC experiment performed with an acquisition time of 108 ms in t_2 and no additional relaxation delay, the full transfer corresponding to a 90° rotation by an average $^1J_{CH}$ of 145 Hz is achieved by the delay $\Delta = 1.72$ ms. We determined an optimal Ernst angle of $\beta' = 63°$ for menthol in $CDCl_3$, which corresponds to a coupling delay of $\Delta' = 1.2$ ms in the INEPT step. Therefore, for the multiplicity edited ASAP-HSQC under the same experimental conditions, $\beta' = 117°$, which corresponds to a transfer delay $\Delta^* = 2.24$ ms, is used.

The resulting sequence allows the acquisition of multiplicity edited HSQC spectra in only few seconds in combination with the use of NUS. An example of a spectrum is shown in Fig. 7. It

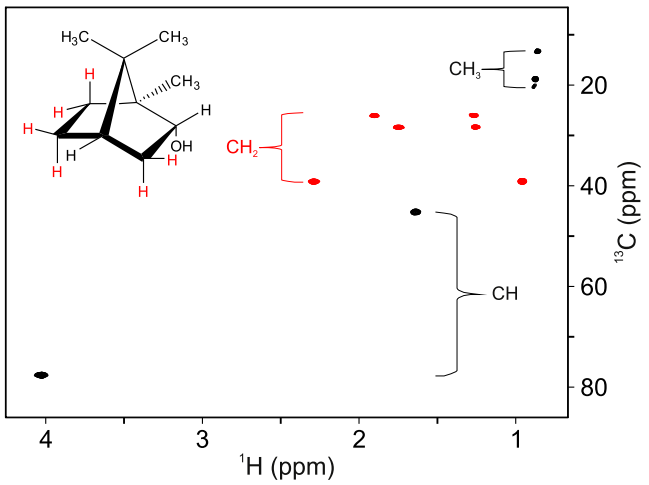

Fig. 7. Multiplicity-edited ASAP-HSQC spectrum of borneol in $CDCl_3$. An expanded matrix of 256 × 128 data points corresponding to acquisition times of 56.2 and 5 ms, respectively, was recorded. Due to 25 % NUS the number of actually acquired points in the indirect dimension is reduced to 32. The experiment was acquired using 1 scan per t_1 increment and 4 dummy scans in altogether 3 s.

was recorded using borneol as a reference sample in an overall experiment duration of only 3 s.

5.2. ASAP-HSQC and water suppression

In Fig. 1D a pulse sequence of the ASAP-HSQC especially designed for water suppression is presented. The sequence uses additional gradients to dephase the strong proton magnetization of the solvent in the *xy*-plane whenever possible. Furthermore, weak bipolar gradient pairs during the t_1 period are applied to reduce the effect of radiation damping [34].

The sequence is implemented using hard pulses due to their shorter length compared to the broadband pulses applied in the other experiments. As a result, signal intensities will be reduced for larger chemical shift offsets, but radiation damping is minimized. The sequence allows the acquisition of complete $^{1}H,^{13}C$-HSQC spectra on water samples within seconds. Fig. 8 shows two HSQC spectra of a 100 mM sucrose sample and a 2 mM standard sucrose sample at natural abundance in a mixture of 90% H_2O and 10% D_2O, which have been recorded in 7s and 15 s, respectively. While the more concentrated sample shows a beautiful suppression of water, the low concentration of the 2 mM standard sample, corresponding to an effective carbon concentration of only 22 μM, demonstrates the limit. Still, the desired signals are clearly visible next to the stronger residual water artefacts that are well within the tolerable dynamic range.

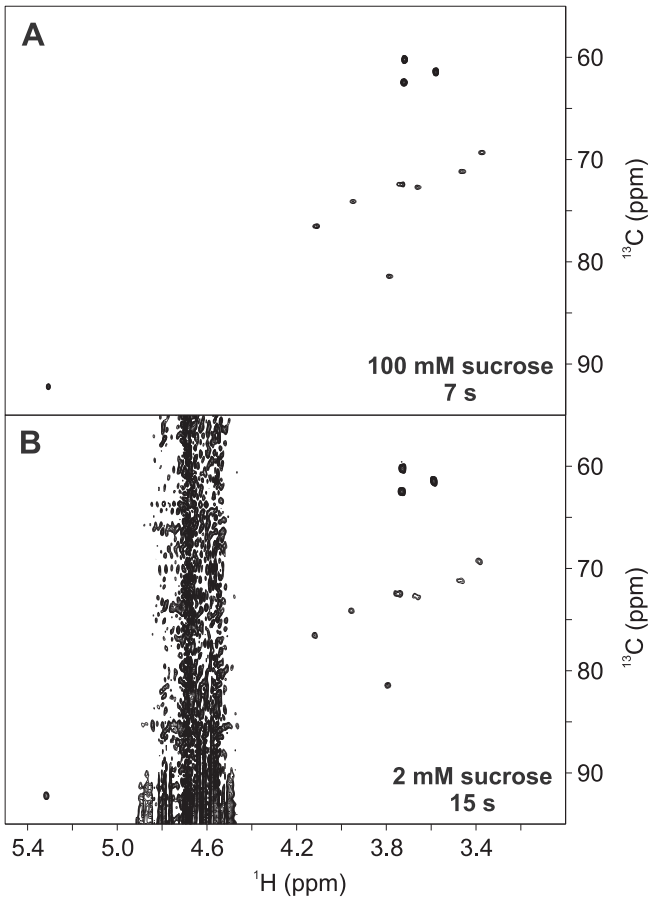

Fig. 8. ASAP-HSQC spectra at natural abundance of a 100 mM (A) and a 2 mM (B) sucrose sample in 90% H_2O/10% D_2O using the pulse sequence introduced in Fig. 1D. In both spectra expanded matrices consisting of 512 × 128 data points, corresponding to acquisition times of 85.4 and 7.07 ms, were used. In spectrum A the number of actually acquired points in the ^{13}C-dimension was reduced to 32 points using non-uniform sampling. In both experiments 1 scan and 4 dummy scans were performed with a resulting experiment time of 7 s (A) and 15 s (B).

Compared to the application of water flip-back pulses [54–56], the method used in the sequence shown in Fig. 1D to control the solvent magnetization is not frequency band selective. Thus, also signals near the solvent peak can in principle be identified.

5.3. CLIP-ASAP-HSQC for coupling measurement

Recently, two of the authors published the CLIP-ASAP-HSQC and the CLIP-ALSOFAST-HSQC experiments for the fast measurement of heteronuclear one-bond couplings from ω_2-coupled $^{1}H,^{13}C$ correlation spectra [43]. The pulse sequence which combines the fast acquisition of the ASAP-HSQC [1] and the clean inphase doublets of the CLIP-HSQC [57] has been revised in a symmetrized version. The core of the CLIP-ASAP-HSQC sequence displayed in Fig. 1 is again based on the ASAP-HSQC sequence. The essential difference is the omittance of heteronuclear decoupling and the additional carbon 90° pulse directly before the acquisition period (see Fig. 1A and B). The absence of heteronuclear decoupling allows heteronuclear antiphase contributions to affect the spectrum by causing phase distortions. They arise from mismatched INEPT back transfer delays, as this is always a compromise averaging between different coupling constants. The 90° pulse removes the phase distortions from the spectrum by converting corresponding terms into undetectable multi quantum coherence, enabling highly accurate measurement of one-bond coupling constants [58]. The spectra resulting from the already-published and from the revised pulse sequence are compared in Fig. 9A and B. The adapted symmetrized sequence shows better spectral quality. Using the same contour levels to display the spectra, the spectrum of Fig. 9B originating from the symmetrized CLIP-ASAP-HSQC sequence contains fewer artifacts. These conclusions confirm the results discussed earlier in the text.

The CLIP-ASAP-HSQC reveals its full potential when applied to the measurement of residual dipolar couplings (RDCs). One-bond RDCs are very valuable for the enhanced determination of conformation [59–67], relative configuration [68–76], constitution [77], enantiomeric excess in chiral alignment media [78,79] and even improved resolution in case of overlapping signals [80]. To our knowledge, the fastest acquisition of a 2D spectrum from which RDCs were measured [14], was performed in 60 s with the single scan approach using gradient-encoded imaging type schemes [11–13]. As reported earlier [43], with the fast acquisition scheme of the CLIP-ASAP-HSQC we were able to record spectra of partially aligned samples in about 25 s. In combination with non-uniform sampling (NUS) [23,81] the overall experiment time can be further reduced. For best results, the MOCCA-XY16 isotropic mixing sequence [40] designed for efficient isotropic and dipolar mixing is used. In Fig. 9C, a ω_2-coupled HSQC spectrum of a partially aligned 100 mM sucrose sample in stretched PEO is displayed which was recorded using the pulse sequence presented in Fig. 1B in an overall experiment time of 7 s. The close-up of Signal 9 shows the exemplified comparison of the isotropic and the anisotropic spectrum, together with the determined coupling constants. The isotropic spectrum, shown in Fig. S7 in the supporting information, was obtained from a 100 mM sucrose sample in D_2O choosing the same experiment and overall duration. Dipolar couplings were derived by comparing the splittings obtained from the isotropic and the anisotropic spectra (see Table S1 in the supporting information). For signal C4-H4, overlap with the PEODA gel signal prevented extraction. The doublets of signals C8-H8 and C10-H10 are noticeably asymmetric in the anisotropic spectrum due to strong coupling with neighboring ^{12}C-bound protons and coupling extraction in this case is unreliable. However, in general and considering the measurement uncertainty, the coupling constants are in agreement with data obtained in earlier works [43].

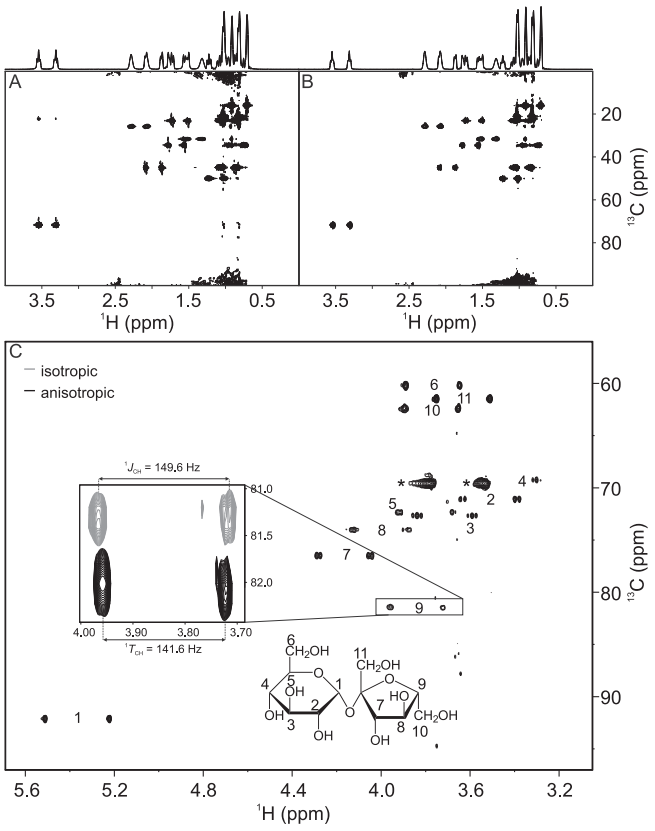

Fig. 9. ω_2-coupled HSQC spectra of menthol in $CDCl_3$ using the original CLIP-ASAP-HSQC [43] (A) and the symmetrized CLIP-ASAP-HSQC (B). The spectra were recorded with 512 × 128 data points, corresponding to acquisition times of 106.8 and 4.2 ms for the two dimensions. For the displayed spectra a DIPSI-2 isotropic mixing sequence of 34.53 ms duration was used. 1 scan per t_1 increment and 4 dummy scans were acquired in overall experiment times of 21 s. The spectra were processed to a total of 1024 × 256 points using zero filling and linear prediction in both dimensions with a resulting resolutions of 2.3 Hz in ω_2 and 58.8 Hz in ω_1. Matching the results shown in Fig. 2, the application of the adapted symmetrized sequence shows better performance regarding the spectral quality. (C) ω_2-coupled CLIP-ASAP-HSQC spectrum of a partially aligned sucrose sample in a stretched PEODA/D_2O gel using the MOCCA-XY16 sequence for isotropic mixing in between scans [40,41]. For the spectrum an expanded matrix of 512 × 128 data points and spectral widths of 1799 and 7540 Hz, corresponding to acquisition times of 142.3 and 8.5 ms for the two dimensions, was recorded. Due to 25 % NUS the number of actually acquired points in the indirect dimension is reduced to 32. The experiment was acquired using 1 scan per t_1 increment and 4 dummy scans in an overall experiment time of 7 s. The spectrum was reconstructed using compressed sensing. In addition, linear prediction as well as zero filling by a factor of 2 in both dimensions was applied. Signals marked with asterisks originate from the alignment medium. The close-up of Signal 9 shows the comparison of the anisotropic (black) and an isotropic 100 mM sucrose (grey) sample with the coupling constants determined from the spectra. The signal originating from the isotropic sample was shifted to graphically facilitate the identification of the spectral differences. Details concerning sample preparation, the spectrum of the isotropic sample and a table with $^1J_{CH}$ and $^1T_{CH}$ coupling values and maximum error estimates are given in the supporting information. Acquisition and processing parameters for the isotropic spectrum equal the settings described for the anisotropic sample.

5.4. ASAP-HSQC and homonuclear BIRD decoupling

The pure shift CLIP-RESET-HSQC allows the acquisition of $^1J_{CH}$-coupled HSQC spectra in ω_2 with broadband ^{1}H,^{1}H decoupling for determination of $^1J_{CH}$ couplings and RDCs with highest precision [82,83]. This is achieved by adding a pseudo dimension encoded by an incremented time period t_2. In the center of this period, a BIRD^d filter is applied which selectively inverts the proton spins directly bound to ^{13}C. The other protons remain unperturbed and thus the evolution of ^{1}H,^{1}H couplings is refocused.

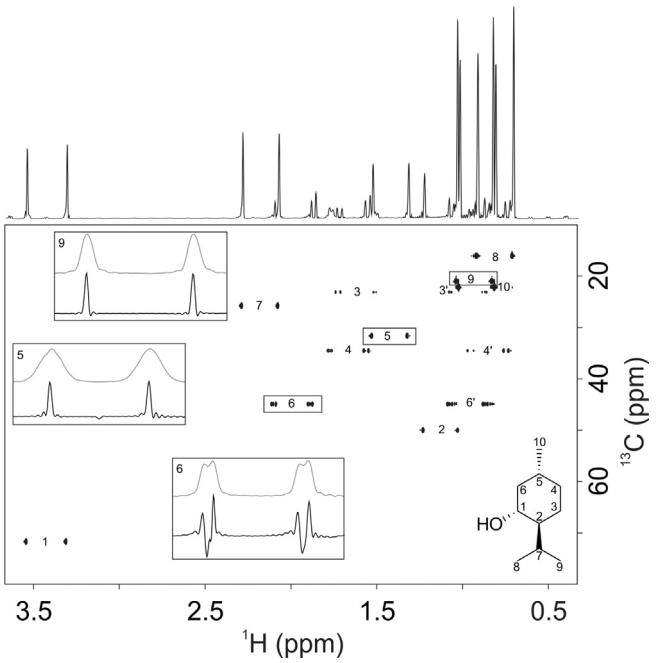

Fig. 10. ω_2-$^1J_{CH}$-coupled HSQC spectrum of menthol with broadband ^{1}H,^{1}H decoupling. Three signals are highlighted. Signal 5 shows a CH group, Signal 6 is a CH_2 group and Signal 9 displays a CH_3 group. To clarify the advantages, respective projections of the CLIP-ASAP-HSQC (for details see Fig. 9B) are displayed in grey (scaled to equal signal height). Clearly, the reduced multiplet width due to the removed splitting of homonuclear decoupling is visible. While most simple doublets result for CH and CH_3 groups, the BIRD filter cannot decouple the geminal coupling as both protons are bound to the same carbon, thus leading to the disturbed lineshape of the CH_2 group. A constant time version [82] or perfect echoing [85] could reduce also these multiplets to doublets. The spectrum was recorded using 648 × 128 data points corresponding to acquisition times of 162 and 6.06 ms. The duration of each FID chunk was set to 16 ms. Two scans per t_1 increment and 16 dummy scans at the beginning of the experiment were performed. The total experimental duration was 13 min and 17 s.

To achieve broadband homonuclear decoupled spectra, the FID has to be recorded in chunks. The duration of each chunk is kept short such that the evolution of ^{1}H,^{1}H-couplings can be neglected. Each t_2-increment represents one chunk. In the end, the chunks are combined to an interferogram, a complete and broadband-^{1}H,^{1}H-decoupled FID (for a review of homonuclear decoupling methods see e.g. Ref. [84]).

The acquisition of up to 40 chunks per FID poses a high time demand and a faster acquisition scheme would be highly desirable. Fig. 1E shows an ASAP version of the experiment consisting of a slightly modified symmetrized CLIP-ASAP-HSQC experiment with the RESET acquisition scheme at the end. Due to the acquisition scheme with the BIRD filter, the Ernst angle-type excitation of anti-phase coherence has to be modified in the same way as for the multiplicity-edited ASAP-HSQC. The high repetition rate allows the acquisition of pseudo 3D spectra in less than 20 min without compromises in terms of spectral quality and resolution (see Fig. 10).

It should be noted that in the process of writing up the manuscript also a real-time pure shift CLIP-RESET-HSQC experiment with only slight errors in coupling measurement has been published [86]. It should also be noted that even CH_2-groups could be simplified if a constant time version of the experiment [82] or perfect echoing [85] would be used. However, as both schemes would result in increased experimental time and reduced signal intensities, we did not implement corresponding experiments.

6. RF-power considerations

Like in all rapid NMR experiments with very fast repetition rates, the corresponding high duty cycle of the experiment has to be considered, which in principle can cause hardware damage. The lock level as a very indirect measure and in the case of cryogenically cooled probeheads the cryoprobe coil heater as a more direct measure can be used to monitor the impact of rf-irradiation. Cryogenically cooled probeheads seem to be particularly tolerant to high rf-power levels and duty cycles [87] and we consequently did not observe problems with any of the pulse sequences introduced here. As the tolerance to duty cycles differs strongly between different probeheads, a general rule for viable duty cycles cannot be given. The applied rf-power though may be significantly reduced by a different choice of decoupling and isotropic mixing sequences, but in the end it might still be necessary to increase the recovery delay in cases where an available probehead is not sufficiently power-tolerant. In the supporting information a useful collection of coarse guidelines for the experimental setup of ASAP- and ALSOFAST-HSQC experiments is given. However, a direct measure for rf-power tolerance is unfortunately not yet available for arbitrary probeheads.

7. Experimental

All shown spectra were recorded on a 600 MHz Bruker Avance III spectrometer equipped with a $^{1}H,^{13}C,^{15}N$-TCI cryogenically cooled probehead optimized for ^{1}H-detection at a temperature of 300 K. For Hartmann-Hahn mixing a DIPSI-2 sequence with rf-amplitude of 5 kHz and a mixing time of 34.54 ms or a MOCCA-XY16 sequence using 180° pulses of 40 μs length and an overall duration of 26.88 ms was used. Processing was achieved using Bruker TopSpin 3.2. When mentioned in corresponding figure captions, complex linear forward prediction of time domain data was utilized. After zero filling to twice the number of data points in both dimensions and apodization using an exponential window function, 2D spectra were Fourier transformed. If possible, we used offset-compensated OCT-derived shaped pulses on both channels in the ASAP-HSQC-based experiments. For details see figure caption of Fig. 1. In all cases, complex data acquisition in the indirect dimension was achieved using the echo/antiecho method.

Spectra were recorded using various model samples: a 500 mM menthol/$CDCl_3$ sample, a 200 mM maltose/D_2O sample, a 10 mM sucrose/D_2O sample, a 100 mM and a 2 mM Bruker standard sample of sucrose in 90% H_2O/10% D_2O, and a 100 mM borneol/$CDCl_3$ sample. All solutes were used at natural-abundance isotope level. For NUS data the compressed sensing algorithm [88] of TopSpin 3.2 was used in all cases for processing. The optimal value Δ' for a specific sample can be determined by performing parameter optimization experiments with a 1D version of the ASAP-HSQC experiment.

The stretched PEODA gel [89] was prepared using 151.7 mg poly(ethyleneoxide) diacrylate (PEODA) with a molecular weight of 35 kDa, dissolved in 500 μl D_2O. The polymer was crosslinked by adding 1.5 μl of a solution which contained 10% (v/v) of tetramethylethylenediamine (TEMED) in D_2O and 5.0 μl of a solution containing 10% (w/w) of ammonium persulfate (APS) in D_2O. A 100 mM sucrose solution was put on top of the gel to diffuse into it and the readily swollen gel was placed into a silicone tube-based stretching device [81,90–92]. The gel was stretched to an extension factor of $\Xi = 0.5$ calculated according to $\Xi = (L/L_0) - 1$ with L being the length of the stretched gel and L_0 the length of the unstretched gel. A quadrupolar splitting of the deuterium signal of the solvent of $\Delta\nu_Q = 3.4$ Hz at 600 MHz and 300 K was introduced, which corresponds to very weak alignment. Gel homogeneity was checked using ^{2}H spectra with spatial resolution along the z-axis [93]. The scalar one-bond CH couplings were obtained from the corresponding ASAP-CLIP-HSQC spectrum using a 100 mM isotropic solution of sucrose dissolved in D_2O.

8. Conclusion

Previously the ASAP-HSQC and the ALSOFAST-HSQC were introduced as promising new techniques that allow the acquisition of very fast heteronuclear correlation experiments at natural isotope abundance [1,43]. In this article several improvements and extensions to the original sequence as well as considerations concerning sensitivity and applicability are given.

A novel symmetrized sequence of the ASAP/ALSOFAST-HSQC is presented which allows acquisition of spectra with minimal artifacts using the same reduced recovery delays in between scans reported previously. The performance of both symmetrized and original experiments have been compared using hard and OCT-derived broadband pulses, clearly indicating that the symmetrized sequence featuring broadband pulses results in best spectral quality. The enhancement by the isotropic mixing period in the ASAP experiment is shown and a theoretical treatment concerning sensitivity of the ASAP-HSQC and ALSOFAST-HSQC vs. conventional HSQC experiments has been initiated. As a first qualitative result it is shown that for proton-rich small molecules highest signal-to-noise ratio per experiment time is achieved in the ASAP-HSQC with short interscan delays, while for molecules without extended coupling networks the ALSOFAST-HSQC works best. The conventional HSQC is only competitive with interscan delays that are on the order of the relaxation time T_1. Combining the ASAP method with further time saving techniques like non-uniform sampling, zero filling, and linear prediction, complete $^{1}H,^{13}C$-HSQC spectra can be acquired in as little as two seconds and digital ^{13}C resolutions significantly below 1 Hz can be achieved in a $^{1}H,^{13}C$-ASAP/ALSOFAST-HSQC in less than 10 min. Furthermore, the symmetrized sequence has been extended by a multiplicity editing step to distinguish CH_2 from CH and CH_3 groups; a pulse sequence with enhanced gradient scheme is shown to allow the acquisition of HSQC spectra of water samples in 15 s at natural abundance and concentrations as low as 2 mM; the compatibility of the approach with BIRD-based $^{1}H,^{1}H$-homonuclear decoupling schemes as well as the application of symmetrized CLIP-ASAP-HSQC experiments with overall durations below 10 s for RDC measurement in weakly aligned samples has been shown. In the end, potential issues with the high duty cycle of the experiment are briefly discussed, providing coarse guidelines to an experimental setup as supporting information.

Acknowledgment

J.B. and M.R.M.K. thank the Fonds der Chemischen Industrie for a PhD fellowship. All authors thank the HGF programme BIFTM as well as the Deutsche Forschungsgemeinschaft (instrumentation facility Pro^{2}NMR, LU 835/13-1, SFB 1176 projects A1 (D.S.S. and J. B.) and Q2 (B.L.)) for financial support. The authors also thank Thomas Gloge for the help with the preparation of the PEODA sample and Tony Reinsperger for support concerning CLIP-RESET experiments.

Appendix A. Supplementary material

Supplementary data associated with this article can be found, in the online version, at http://dx.doi.org/10.1016/j.jmr.2017.05.012.

References

[1] D. Schulze-Sünninghausen, J. Becker, B. Luy, Rapid heteronuclear single quantum correlation NMR spectra at natural abundance, J. Am. Chem. Soc. 136 (2014) 1242–1245.
[2] G. Bodenhausen, D.J. Ruben, Natural abundance N-15 NMR by enhanced heteronuclear spectroscopy, Chem. Phys. Lett. 69 (1980) 185–189.
[3] P. Schanda, B. Brutscher, Very fast two-dimensional NMR spectroscopy for real-time investigation of dynamic events in proteins on the time scale of seconds, J. Am. Chem. Soc. 127 (2005) 8014–8015.
[4] P. Schanda, Ē. Kupče, B. Brutscher, SOFAST-HMQC experiments for recording two-dimensional heteronuclear correlation spectra of proteins within a few seconds, J. Biomol. NMR 33 (2005) 199–211.
[5] P. Schanda, V. Forge, B. Brutscher, HET-SOFAST NMR for fast detection of structural compactness and heterogeneity along polypeptide chains, Magn. Reson. Chem. 44 (2006) S177–S184.
[6] T. Kern, P. Schanda, B. Brutscher, Sensitivity-enhanced IPAP-SOFAST-HMQC for fast-pulsing 2D NMR with reduced radiofrequency load, J. Magn. Reson. 190 (2008) 333–338.
[7] E. Lescop, P. Schanda, B. Brutscher, A set of BEST triple-resonance experiments for time-optimized protein resonance assignment, J. Magn. Reson. 187 (2007) 163–169.
[8] P. Schanda, H. Van Melckebeke, B. Brutscher, Speeding up three-dimensional protein NMR experiments to a few minutes, J. Am. Chem. Soc. 128 (2006) 9042–9043.
[9] J. Farjon, J. Boisbouvier, P. Schanda, A. Pardi, J.-P. Simorre, B. Brutscher, Longitudinal-relaxation-enhanced NMR experiments for the study of nucleic acids in solution, J. Am. Chem. Soc. 131 (2009) 8571–8577.
[10] M. Deschamps, I.D. Campbell, Cooling overall spin temperature: protein NMR experiments optimized for longitudinal relaxation effects, J. Magn. Reson. 178 (2006) 206–211.
[11] L. Frydman, T. Scherf, A. Lupulescu, The acquisition of multidimensional NMR spectra within a single scan, Proc. Natl. Acad. Sci. U.S.A. 99 (2002) 15858–15862.
[12] P. Pelupessy, Adiabatic single scan two-dimensional NMR spectrocopy, J. Am. Chem. Soc. 125 (2003) 12345–12350.
[13] A. Tal, L. Frydman, Single-scan multidimensional magnetic resonance, Prog. Nucl. Magn. Reson. Spectrosc. 57 (2010) 241–292.
[14] P. Giraudeau, T. Montag, B. Charrier, C.M. Thiele, Fast access to residual dipolar couplings by single-scan 2D NMR in oriented media, Magn. Reson. Chem. 50 (2012) 53–57.
[15] R.R. Ernst, G. Bodenhausen, A. Wokaun, Principles of Nuclear Magnetic Resonance, Oxford University Press, 1987.
[16] T. Diercks, M. Daniels, R. Kaptein, Extended flip-back schemes for sensitivity enhancement in multidimensional HSQC-type out-and-back experiments, J. Biomol. NMR 33 (2005) 243–259.
[17] Ē. Kupče, R. Freeman, Fast multidimensional NMR by polarization sharing, Magn. Reson. Chem. 45 (2007) 2–4.
[18] J. Furrer, A robust, sensitive, and versatile HMBC experiment for rapid structure elucidation by NMR: IMPACT-HMBC, Chem. Commun. 46 (2010) 3396–3398.
[19] B. Vitorge, G. Bodenhausen, P. Pelupessy, Speeding up nuclear magnetic resonance spectroscopy by the use of SMAll Recovery Times – SMART NMR, J. Magn. Reson. 207 (2010) 149–152.
[20] G.E. Wagner, P. Sakhaii, W. Bermel, K. Zangger, Monitoring fast reactions by spatially-selective and frequency-shifted continuous NMR spectroscopy: application to rapid-injection protein unfolding, Chem. Commun. 49 (2013) 3155–3157.
[21] L. Mueller, Alternate HMQC experiments for recording HN and HC-correlation spectra in proteins at high throughput, J. Biomol. NMR 42 (2008) 129–137.
[22] J.R. Garbow, D.P. Weitekamp, A. Pines, Bilinear rotation decoupling of homonuclear scalar interactions, Chem. Phys. Lett. 93 (1982) 504–509.
[23] H.S. Atreya, T. Szyperski, H. Hauptman, G-matrix Fourier Transform NMR spectroscopy for complete protein resonance assignment, Proc. Natl. Acad. Sci. U.S.A. 101 (2004) 9642–9647.
[24] D. Marion, Fast acquisition of NMR spectra using Fourier transform of non-equispaced data, J. Biomol. NMR 32 (2005) 141–150.
[25] K. Kobzar, S. Ehni, T.E. Skinner, S.J. Glaser, B. Luy, Exploring the limits of broadband 90 degrees and 180 degrees universal rotation pulses, J. Magn. Reson. 225 (2012) 142–160.
[26] K. Kobzar, T.E. Skinner, N. Khaneja, S.J. Glaser, B. Luy, Exploring the limits of broadband excitation and inversion pulses, J. Magn. Reson. 170 (2004) 236–243.
[27] K. Kobzar, T.E. Skinner, N. Khaneja, S.J. Glaser, B. Luy, Exploring the limits of broadband excitation and inversion: II. Rf-power optimized pulses, J. Magn. Reson. 194 (2008) 58–66.
[28] T.E. Skinner, K. Kobzar, B. Luy, M.R. Bendall, W. Bermel, N. Khaneja, S.J. Glaser, Optimal control design of constant amplitude phase-modulated pulses: application to calibration-free broadband excitation, J. Magn. Reson. 179 (2006) 241–249.
[29] T.E. Skinner, T.O. Reiss, B. Luy, N. Khaneja, S.J. Glaser, Application of optimal control theory to the design of broadband excitation pulses for high-resolution NMR, J. Magn. Reson. 163 (2003) 8–15.
[30] T.E. Skinner, T.O. Reiss, B. Luy, N. Khaneja, S.J. Glaser, Reducing the duration of broadband excitation pulses using optimal control with limited RF amplitude, J. Magn. Reson. 167 (2004) 68–74.
[31] B. Luy, K. Kobzar, T.E. Skinner, N. Khaneja, S.J. Glaser, Construction of universal rotations from point-to-point transformations, J. Magn. Reson. 176 (2005) 179–186.
[32] T.E. Skinner, N.I. Gershenzon, M. Nimbalkar, W. Bermel, B. Luy, S.J. Glaser, New strategies for designing robust universal rotation pulses: application to broadband refocusing at low power, J. Magn. Reson. 216 (2012) 78–87.
[33] S. Ehni, B. Luy, BEBEtr and BUBI: J-compensated concurrent shaped pulses for 1H–13C experiments, J. Magn. Reson. 232 (2013) 7–17.
[34] V. Sklenář, Suppression of radiation damping in multidimensional NMR Experiments using magnetic field gradients, J. Magn. Reson. A 114 (1995) 132–135.
[35] T.E. Skinner, T.O. Reiss, B. Luy, N. Khaneja, S.J. Glaser, Tailoring the optimal control cost function to a desired output: application to minimizing phase errors in short broadband excitation pulses, J. Magn. Reson. 172 (2005) 17–23.
[36] S. Ehni, B. Luy, A systematic approach for optimizing the robustness of pulse sequence elements with respect to couplings, offsets, and B_1-field inhomogeneities (COB), Magn. Reson. Chem. 50 (2012) S63–S72.
[37] S. Ehni, B. Luy, Robust INEPT and refocused INEPT transfer with compensation of a wide range of couplings, offsets, and B_1-field inhomogeneities (COB3), J. Magn. Reson. 247 (2014) 111–117.
[38] A.J. Shaka, P.B. Barker, R. Freeman, Computer-optimized decoupling scheme for wideband applications and low-level operation, J. Magn. Reson. 64 (1985) 547–552.
[39] A.J. Shaka, C.J. Lee, A. Pines, Iterative schemes for bilinear operators; application to spin decoupling, J. Magn. Reson. 77 (1988) 274–293.
[40] J. Furrer, F. Kramer, J. Marino, S. Glaser, B. Luy, Homonuclear Hartmann-Hahn transfer with reduced relaxation losses by use of the MOCCA-XY16 multiple pulse sequence, J. Magn. Reson. 166 (2004) 39–46.
[41] F. Kramer, W. Peti, C. Griesinger, S.J. Glaser, Optimized homonuclear Carr–Purcell-type dipolar mixing Sequences, J. Magn. Reson. 149 (2001) 58–66.
[42] D. Marion, K. Wüthrich, Application of phase sensitive two-dimensional correlated spectroscopy (COSY) for measurements of 1H–1H spin-spin coupling constants in proteins, Biochem. Bioph. Res. Commun. 113 (1983) 967–974.
[43] J. Becker, B. Luy, CLIP–ASAP–HSQC for fast and accurate extraction of one-bond couplings from isotropic and partially aligned molecules, Magn. Reson. Chem. 53 (2015) 878–885.
[44] B. Luy, S. Glaser, Superposition of scalar and residual dipolar couplings: analytical transfer functions for three spins 1/2 under cylindrical mixing conditions, J. Magn. Reson. 148 (2001) 169–181.
[45] D.M. Taylor, A. Ramamoorthy, Analysis of dipolar-coupling-mediated coherence transfer in a homonuclear two spin-1/2 solid-state system, J. Magn. Reson. 141 (1999) 18–28.
[46] O. Schedletzky, S.J. Glaser, Analytical coherence-transfer functions for the general AMX spin system under isotropic mixing, J. Magn. Reson. A 123 (1996) 174–180.
[47] B. Luy, O. Schedletzky, S. Glaser, Analytical polarization transfer functions for four coupled spins 1/2 under isotropic mixing conditions, J. Magn. Reson. 138 (1999) 19–27.
[48] M. Rance, Sign reversal of resonances via isotropic mixing in NMR spectroscopy, Chem. Phys. Lett. 154 (1989) 242–247.
[49] B. Luy, S.J. Glaser, Negative polarization transfer between a spin 1/2 and a spin 1, Chem. Phys. Lett. 323 (2000) 377–381.
[50] R.R. Ernst, G. Bodenhausen, A. Wokaun, Principles of Nuclear Magnetic Resonance in One and Two Dimensions, Oxford University Press, New York, 1987.
[51] X. Zhang, C. Wang, ^{1}H-Detected editable heteronuclear multiple-quantum correlation experiment at natural abundance, J. Magn. Reson. 91 (1991) 618–623.
[52] W. Willker, D. Leibfritz, R. Kerssebaum, W. Bermel, Gradient selection in inverse heteronuclear correlation spectroscopy, Magn. Reson. Chem. 31 (1993) 287–292.
[53] D.G. Davis, Improved multiplet editing of proton-detected, heteronuclear shift-correlation spectra, J. Magn. Reson. 91 (1991) 665–672.
[54] S. Grzesiek, A. Bax, The importance of not saturating water in protein NMR. Application to sensitivity enhancement and NOE measurements, J. Am. Chem. Soc. 115 (1993) 12593–12594.
[55] J. Stonehouse, G.L. Shaw, J. Keeler, E.D. Laue, Minimizing sensitivity losses in gradient-selected 15N–1H HSQC spectra of proteins, J. Magn. Reson. A 107 (1994) 178–184.
[56] S. Mori, C. Abeygunawardana, M.O. Johnson, P.C.M. Van Zijl, Improved sensitivity of HSQC spectra of exchanging protons at short interscan delays using a new fast HSQC (FHSQC) detection scheme that avoids water saturation, J. Magn. Reson. B 108 (1995) 94–98.
[57] A. Enthart, J.C. Freudenberger, J. Furrer, H. Kessler, B. Luy, The CLIP/CLAP-HSQC: pure absorptive spectra for the measurement of one-bond couplings, J. Magn. Reson. 192 (2008) 314–322.
[58] J. Yan, A.D. Kline, H. Mo, M.J. Shapiro, E.R. Zartler, A novel method for the determination of stereochemistry in six-membered chairlike rings using residual dipolar couplings, J. Org. Chem. 68 (2003) 1786–1795.
[59] V.M. Sánchez-Pedregal, R. Santamaría-Fernández, A. Navarro-Vázquez, Residual dipolar couplings of freely rotating groups in small molecules. Stereochemical assignment and side-chain conformation of 8-phenylmenthol, Org. Lett. 11 (2009) 1471–1474.

[60] C. Gayathri, M.C. de la Fuente, B. Luy, R.R. Gil, A. Navarro-Vázquez, Probing heterocycle conformation with residual dipolar couplings, Chem. Commun. 46 (2010) 5879–5881.
[61] P. Trigo-Mouriño, R. Santamaría-Fernández, V.M. Sánchez-Pedregal, A. Navarro-Vázquez, Conformational analysis of an isoquinolinium hydrochloride in water using residual dipolar couplings, J. Org. Chem. 75 (2010) 3101–3104.
[62] A. Schuetz, T. Murakami, N. Takada, J. Junker, M. Hashimoto, C. Griesinger, RDC-enhanced NMR spectroscopy in structure elucidation of sucro-neolambertellin, Angew. Chem. Int. Ed. 47 (2008) 2032–2034.
[63] S. Weigelt, T. Huber, F. Hofmann, M. Jost, M. Ritzefeld, B. Luy, C. Freudenberger, Z. Majer, E. Vass, J.-C. Greie, L. Panella, B. Kaptein, Q.B. Broxterman, H. Kessler, K. Altendorf, M. Hollosi, N. Sewald, Synthesis and conformational analysis of efrapeptins, Chem. Eur. J. 18 (2012) 478–487.
[64] M. Martin-Pastor, C.A. Bush, Conformational studies of human milk oligosaccharides using 1H–13C one-bond NMR residual dipolar couplings, Biochemistry 39 (2000) 4674–4683.
[65] M. Martin-Pastor, A. Canales-Mayordomo, J. Jiménez-Barbero, NMR experiments for the measurement of proton–proton and carbon–carbon residual dipolar couplings in uniformly labelled oligosaccharides, J. Biomol. NMR 26 (2003) 345–353.
[66] T.N. Pham, S.L. Hinchley, D.W.H. Rankin, T. Liptaj, D. Uhrin, Determination of sugar structures in solution from residual dipolar coupling constants: methodology and application to methyl β-D-xylopyranoside, J. Am. Chem. Soc. 126 (2004) 13100–13110.
[67] J. Klages, C. Neubauer, M. Coles, H. Kessler, B. Luy, Structure refinement of cyclosporin A in chloroform by using RDCs measured in a stretched PDMS-Gel, ChemBioChem 6 (2005) 1672–1678.
[68] C. Aroulanda, V. Boucard, F. Guibé, J. Courtieu, D. Merlet, Weakly oriented liquid-crystal NMR solvents as a general tool to determine relative configurations, Chem. Eur. J. 9 (2003) 4536–4539.
[69] A. Mangoni, V. Esposito, A. Randazzo, Configuration assignment in small organic molecules via residual dipolar couplings, Chem. Commun. 154–155 (2003).
[70] J. Yan, F. Delaglio, A. Kaerner, A.D. Kline, H. Mo, M.J. Shapiro, T.A. Smitka, G.A. Stephenson, E.R. Zartler, Complete relative stereochemistry of multiple stereocenters using only residual dipolar couplings, J. Am. Chem. Soc. 126 (2004) 5008–5017.
[71] M.E. García, S. Pagola, A. Navarro-Vázquez, D.D. Phillips, C. Gayathri, H. Krakauer, P.W. Stephens, V.E. Nicotra, R.R. Gil, Stereochemistry determination by powder X-ray diffraction analysis and NMR spectroscopy residual dipolar couplings, Angew. Chem. Int. Ed. 48 (2009) 5670–5674.
[72] A. Schuetz, J. Junker, A. Leonov, O.F. Lange, T.F. Molinski, C. Griesinger, Stereochemistry of sagittamide a from residual dipolar coupling enhanced NMR, J. Am. Chem. Soc. 129 (2007) 15114–15115.
[73] U.M. Reinscheid, M. Köck, C. Cychon, V. Schmidts, C.M. Thiele, C. Griesinger, The absolute configuration of dibromopalau'amine, Eur. J. Org. Chem. 2010 (2010) 6900–6903.
[74] M.J. Riveira, C. Gayathri, A. Navarro-Vázquez, N.V. Tsarevsky, R.R. Gil, M.P. Mischne, Unprecedented stereoselective synthesis of cyclopenta[b]benzofuran derivatives and their characterisation assisted by aligned media NMR and ^{13}C chemical shift *ab initio* predictions, Org. Biomol. Chem. 9 (2011) 3170–3175.
[75] P. Trigo-Mouriño, R. Sifuentes, A. Navarro-Vázquez, C. Gayathri, H. Maruenda, R.R. Gil, Determination of the absolute configuration of 19-OH-(–)-eburnamonine using a combination of residual dipolar couplings, DFT chemical shift predictions, and chiroptics, Nat. Prod. Commun. 7 (2012) 735–738.
[76] D. Intelmann, G. Kummerloewe, G. Haseleu, N. Desmer, K. Schulze, R. Froehlich, O. Frank, B. Luy, T. Hofmann, Structures of storage-induced transformation products of the beer's bitter principles, revealed by sophisticated NMR spectroscopic and LC-MS techniques, Chem. Eur. J. 15 (2009) 13047–13058.
[77] G. Kummerlöwe, S.L. Grage, C.M. Thiele, I. Kuprov, A.S. Ulrich, B. Luy, Variable angle NMR spectroscopy and its application to the measurement of residual chemical shift anisotropy, J. Magn. Reson. 209 (2011) 19–30.
[78] B. Luy, Distinction of enantiomers by NMR spectroscopy using chiral orienting media, J. Indian Inst. Sci. 90 (2010) 119–132.
[79] P. Lesot, J. Courtieu, Natural abundance deuterium NMR spectroscopy: developments and analytical applications in liquids, liquid crystals and solid phases, Prog. Nucl. Magn. Reson. Spectrosc. 55 (2009) 128–159.
[80] J. Furrer, M. John, H. Kessler, B. Luy, *J*-Spectroscopy in the presence of residual dipolar couplings: determination of one-bond coupling constants and scalable resolution, J. Biomol. NMR 37 (2007) 231–243.
[81] G. Kummerlöwe, E.F. McCord, S.F. Cheatham, S. Niss, R.W. Schnell, B. Luy, Tunable alignment for all polymer gel/solvent combinations for the measurement of anisotropic NMR parameters, Chem. Eur. J. 16 (2010) 7087–7089.
[82] T. Reinsperger, B. Luy, Homonuclear BIRD-decoupled spectra for measuring one-bond couplings with highest resolution: CLIP/CLAP-RESET and constant-time-CLIP/CLAP-RESET, J. Magn. Reson. 239 (2014) 110–120.
[83] I. Timári, L. Kaltschnee, A. Kolmer, R.W. Adams, M. Nilsson, C.M. Thiele, G.A. Morris, K.E. Kövér, Accurate determination of one-bond heteronuclear coupling constants with "pure shift" broadband proton-decoupled CLIP/CLAP-HSQC experiments, J. Magn. Reson. 239 (2014) 130–138.
[84] L. Castañar, T. Parella, Broadband ^{1}H homodecoupled NMR experiments: recent developments, methods and applications, Magn. Reson. Chem. 53 (2015) 399–426.
[85] L. Kaltschnee, A. Kolmer, I. Timári, V. Schmidts, R.W. Adams, M. Nilsson, K.E. Kövér, G.A. Morris, C.M. Thiele, "Perfecting" pure shift HSQC: full homodecoupling for accurate and precise determination of heteronuclear couplings, Chem. Commun. 50 (2014) 15702–15705.
[86] I. Timári, L. Kaltschnee, M.H. Raics, F. Roth, N.G.A. Bell, R.W. Adams, M. Nilsson, D. Uhrin, G.A. Morris, C.M. Thiele, K.E. Kövér, Real-time broadband proton-homodecoupled CLIP/CLAP-HSQC for automated measurement of heteronuclear one-bond coupling constants, RSC Adv. 6 (2016) 87848–87855.
[87] D. Ban, A.D. Gossert, K. Giller, S. Becker, C. Griesinger, D. Lee, Exceeding the limit of dynamics studies on biomolecules using high spin-lock field strengths with a cryogenically cooled probehead, J. Magn. Reson. 221 (2012) 1–4.
[88] K. Kazimierczuk, V.Y. Orekhov, Accelerated NMR spectroscopy by using compressed sensing, Angew. Chem. Int. Ed. 50 (2011) 5556–5559.
[89] C. Merle, G. Kummerlöwe, F. Halbach, C. Lierse von Gostomski, J. Höpfner, T. Beskers, M. Wilhelm, B. Luy, Crosslinked poly(ethylene oxide) as a versatile alignment medium for the measurement of residual anisotropic NMR parameters, Angew. Chem. Int. Ed. 52 (2013) 10309–10312.
[90] P.W. Kuchel, B.E. Chapman, N. Müller, W.A. Bubb, D.J. Philp, A.M. Torres, Apparatus for rapid adjustment of the degree of alignment of NMR samples in aqueous media: verification with residual quadrupolar splittings in ^{23}Na and ^{133}Cs spectra, J. Magn. Reson. 180 (2006) 256–265.
[91] G. Kummerlöwe, F. Halbach, B. Laufer, B. Luy, Precise measurement of RDCs in water and DMSO based gels using a silicone rubber tube for tuneable stretching, Open Spectrosc. J. 2 (2008) 29–33.
[92] G. Kummerlöwe, S. Schmitt, B. Luy, Cross-fitting of residual dipolar couplings, The Open Spectrosc. J. 4 (2010) 16–27.
[93] P. Trigo-Mouriño, C. Merle, M.R.M. Koos, B. Luy, R.R. Gil, Probing spatial distribution of alignment by deuterium NMR imaging, Chem. Eur. J. 19 (2013) 7013–7019.